OPEN ACCESS

Energy Efficiency ARTICLE

Harvesting energy from ocean currents: A vortex induced motion energy conversion system

Muk Chen Ong[1,*] and Marek Jan Janocha[1]

*Correspondence: muk.c.ong@uis.no

Received: December 29, 2025; Accepted: April 9, 2026; Published Online: April 21, 2026; https://doi.org/10.59717/j.xinn-energy.2026.100153

GRAPHICAL ABSTRACT

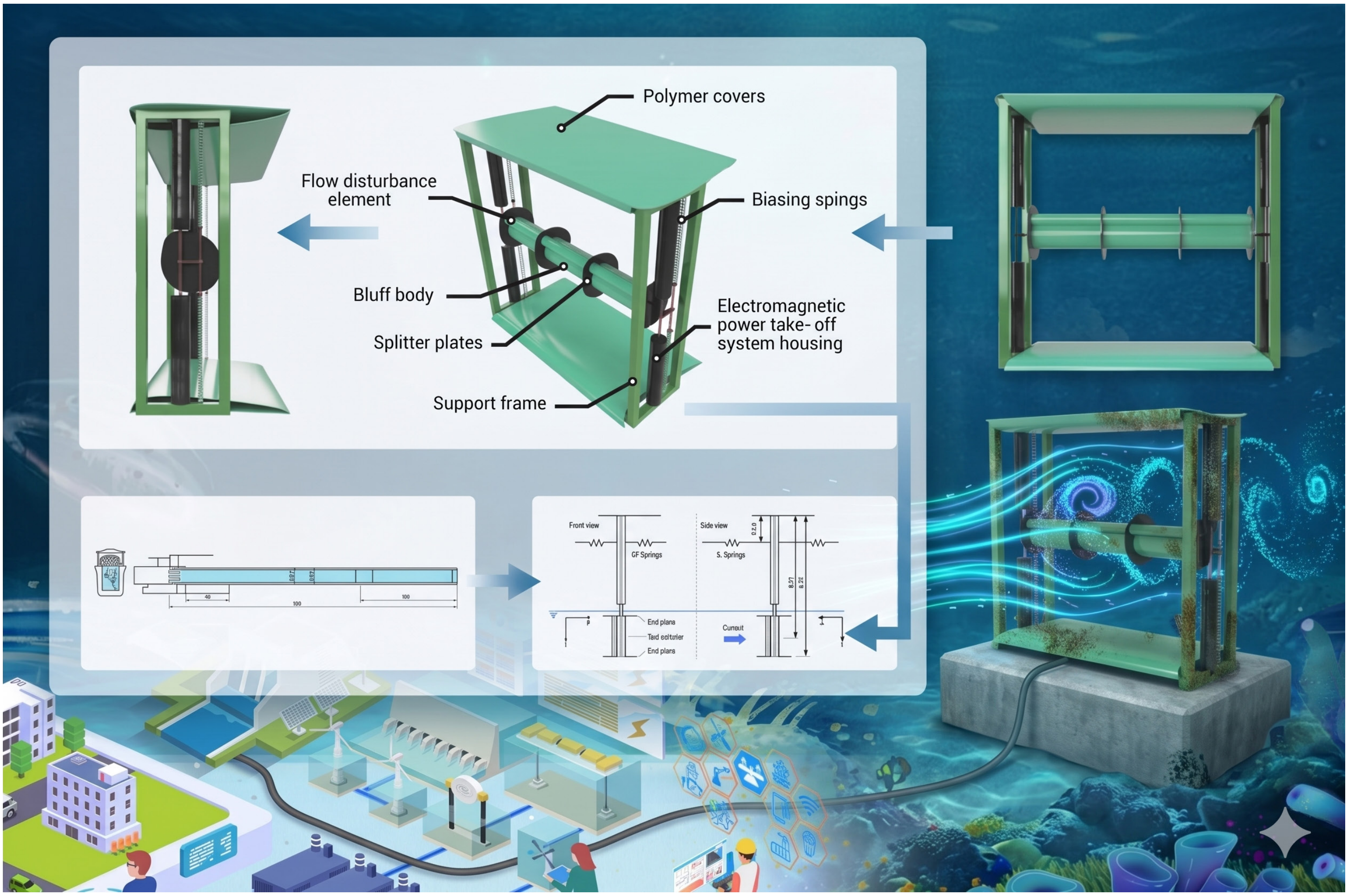

PUBLIC SUMMARY

- A novel VIM device harvests energy from water currents using fluid–structure interaction.
- CFD simulations and experiments validate reliable performance across flow conditions.
- The system works efficiently even near walls, enabling flexible seabed deployment.
- Optimized damping improves energy conversion efficiency significantly.
- Competitive LCOE shows strong potential for coastal and river renewable energy use.

Harvesting energy from ocean currents: A vortex induced motion energy conversion system

Muk Chen Ong[1,*] and Marek Jan Janocha[1]

[1]Department of Mechanical and Structural Engineering and Materials Science, University of Stavanger, Stavanger, Norway

*Correspondence: muk.c.ong@uis.no

Received: December 29, 2025; Accepted: April 9, 2026; Published Online: April 21, 2026; https://doi.org/10.59717/j.xinn-energy.2026.100153

Citation: Ong M. and Janocha M. (2026). Harvesting energy from ocean currents: A vortex induced motion energy conversion system. *The Innovation Energy* **3**:100153.

Hydrokinetic energy harvesting represents a promising direction for sustainable renewable energy generation, leveraging complex fluid-structure interaction (FSI) phenomena to convert water current kinetic energy into electrical power. This study presents a comprehensive investigation of a novel Vortex-Induced Motion (VIM) energy converter designed to maximize power extraction from marine and riverine environments. The research methodology integrates advanced computational fluid dynamics (CFD) modeling with rigorous experimental validation to ensure reliable performance characterization. A CFD model is developed to simulate fluid-structure interactions under diverse hydrodynamic conditions. Experimental verification is conducted through towing tank experiments, enabling robust model calibration and performance assessment. Key findings demonstrate the concept is capable of operating under a wide range of flow velocities, with numerical results confirming minimal performance degradation in near-wall configurations. This characteristic suggests significant potential for seabed deployment across varied marine infrastructures. A detailed parametric analysis systematically evaluates damping configurations, identifying optimal parameters for maximizing energy conversion efficiency. Economic feasibility analysis reveals competitive levelized cost of energy (LCOE) metrics, positioning the proposed energy converter concept as a technically and economically viable renewable energy solution for remote coastal and riverine applications.

INTRODUCTION

Water is Earth's largest natural energy storage medium. It can be viewed as a vast reservoir for renewable energy generatio.[1] Marine hydrokinetic energy (MHE) is the energy contained in moving masses of water such as waves, tides, and currents. According to the International Energy Agency,[2] MHE could theoretically generate 20,000–80,000 TWh of electricity annually, far surpassing the world's current energy consumption of approximately 20,000 TWh.[2] However, despite its promise, harnessing MHE faces significant challenges, including low energy conversion efficiency, high operational thresholds, environmental incompatibilities, and potential disruptions to coastal infrastructure and communities.[1,3]

Ocean currents represent a vast and untapped source of renewable energy, offering a steady and predictable flow of power that can complement other forms of renewable energy such as wind and solar. Unlike intermittent sources, ocean currents are influenced by global thermohaline circulation patterns, wind, and the Earth's rotation, ensuring a consistent energy supply.[4] Large circulation systems such as the Gulf Stream in the Atlantic Ocean and the Kuroshio Current in the Pacific Ocean are particularly promising for large-scale energy extraction.[5,6] Harnessing this energy could significantly contribute to global efforts to transition away from fossil fuels, reduce greenhouse gas emissions, and achieve energy security. Moreover, ocean current energy systems have minimal visual impact, and a lower carbon footprint compared to other renewable technologies, making them a sustainable option for future energy needs.[7]

Ocean current energy harvesting is an emerging engineering field dedicated to the development of technologies to extract kinetic energy from the natural flow of ocean.[8] These technologies typically rely on underwater turbines, which function similarly to wind turbines, but are designed to operate in dense and slow-moving water environments.[9] Devices such as horizontal-axis and vertical-axis turbines, as well as oscillating hydrofoil systems, are commonly used for this purpose.[10,11] Recent advancements in materials science and engineering have led to the development of more durable and efficient turbines that can withstand the harsh marine environment. These systems are often installed on the seabed or suspended in mid-water to capture the energy of predictable and continuous currents, providing a reliable source of renewable energy. Axial-flow turbines, inspired by traditional wind turbines, have been successfully deployed in controlled environments, such as the European Marine Energy Centre (EMEC), demonstrating their ability to operate effectively under steady currents.[1] However, these systems often require precise alignment with flow directions, leading to increased operational complexity. In contrast, cross-flow turbines, such as the Darrieus and Gorlov designs, have shown promise in environments with multidirectional flow patterns. These turbines are capable of harnessing energy from both tidal and riverine flows.[12,13] Moreover, the development of innovative materials and coatings has improved the durability of turbine blades against biofouling and corrosion, two critical issues in marine environments. Advanced anchoring and mooring systems, coupled with remote monitoring capabilities, have further enhanced the operational reliability of ocean current energy systems.

Emerging technologies such as systems exploiting flow-induced vibration (FIV) offer alternative approaches to energy extractio.[14] Flow-Induced Vibration (FIV) encompasses a broad range of phenomena that can be exploited for harvesting energy from fluid flows, leveraging various fluid-elastic instabilities such as vortex-induced vibration (VIV), galloping, flutter, Wake-Induced Oscillations (WIO), and buffeting. These mechanisms have been explored through diverse designs, including flexible plates,[15,16] torsional airfoils,[17,18] and oscillating bluff bodies,[19-22] demonstrating their potential for efficient energy extraction.

VIV plays a central role in ocean current energy conversion by providing the fundamental mechanism through which kinetic energy in a flowing fluid is transferred to a compliant structure. When a bluff body, such as a circular cylinder, is placed in a cross-flow, alternating vortices are shed from its surface (the von Kármán vortex street), creating periodic fluctuating forces. If the body is elastically mounted, these forces induce oscillatory motion. The energy conversion pathway thus follows a clear physical chain: (1) the incoming flow's kinetic energy is converted into coherent vortical structures through boundary layer separation; (2) the vortex shedding process generates alternating pressure forces on the cylinder surface; (3) these forces drive oscillatory structural motion, converting fluid energy into mechanical kinetic and potential energy; and (4) a PTO mechanism extracts this mechanical energy as useful electrical power. The efficiency of this conversion chain depends critically on achieving lock-in (synchronisation between the natural structural frequency and the vortex shedding frequency) which maximises the energy transfer from the fluid to the structure. One of the pioneering devices, is Vortex-Induced Vibration Aquatic Clean Energy (VIVACE) designed by Bernitsas et al. (2006),[23] who have demonstrated high energy conversion efficiencies in experimental settings, offering a low-cost and scalable solution for harnessing ocean current energy.[19] Since its inception, significant progress has been made to enhance FIV harvester efficiency through advancements in electromechanical components and hydroelastic optimization. Research has focused on tuning parameters such as stiffness and mass-damping, implementing multi-oscillator configurations, and modifying the geometrical characteristics of bluff body.[24] For instance, replacing traditional circular cylinders with sharp-edged bluff bodies—such as squares, diamonds, or diamond-oriented squares—effectively circumvents the limited response range of VIV.[19] These geometries can induce powerful galloping instabilities, where oscillation amplitudes increase linearly with flow velocity, or trigger resonance-type responses, leading to a significant boost in power generation and overall energy efficiency.

Xu et al. (2016) investigated power extraction via VIV using a dual-mass system, modeled as a two-degree-of-freedom (2DoF) configuration where fluid forces were derived from forced vibration experiments.[25] Their analysis demonstrated that while maximum theoretical efficiency remains unchanged in an ideal lossless scenario, appropriate tuning of secondary mass and inter-mass stiffness can enhance efficiency when mechanical losses are present. The dual-mass system also exhibited a broader response bandwidth in terms of reduced velocity, highlighting its potential for improving energy harvesting performance.

In tandem configurations, the interaction between upstream and downstream bluff bodies introduces Wake-Induced Oscillations (WIO), where vortex shedding from the upstream cylinder governs the oscillatory behavior of the downstream cylinder. Studies have shown that variations in geometry and spacing can significantly influence lift and drag forces, as well as energy harvesting performance.[26-28] The exploration of tandem arrangements for sharp-edged oscillators remains a promising area for future research, with limited studies addressing their hydroelastic responses in marine environments.[29]

Rashki et al. (2024) investigated the impact of hard marine growth on the energy harvesting efficiency of 2DoF VIV oscillators,[30] which are known for their superior fluctuation amplitudes compared to their one-degree-of-freedom (1DoF) counterparts. Their experimental study, conducted in a towing tank over a Reynolds number range of 6×10^4 to 5.2×10^5 assessed the power output and efficiency of bio-fouled and clean oscillators under optimal piezoelectric coupling. Using additive manufacturing, artificial barnacle colonies were 3D-printed to simulate varying marine growth coverage (33%–100%). Rashki et al. (2024) findings indicate that early-stage biofouling leads to an 81% reduction in energy harvesting performance, with only partial recovery over time, stabilizing at approximately 75% below that of a clean oscillator. Moreover, the presence of hard marine growth negates the performance benefits of the second degree of freedom, causing the 2DoF oscillator to perform 49% worse than a clean 1DoF system.

To fully realize the potential of flow-induced vibration (FIV) energy harvesters, continued research is essential to refine device configurations, enhance hydroelastic responses, and optimize tandem arrangements. Numerical and experimental investigations of sharp-edged bluff bodies in water flows offer valuable insights into improving energy harvesting efficiency. Extending these studies to realistic marine environments can help bridge the gap between conceptual designs and practical implementation, unlocking new opportunities for sustainable energy production.

Vortex-induced vibration (VIV) and broader flow-induced vibration (FIV) phenomena present a promising prospect for renewable hydrokinetic and aerodynamic energy conversion to power remote sensors and low-power microelectronics. However, conventional linear energy harvesters are largely constrained by narrow resonance bandwidths, rendering them inefficient when confronted with the fluctuating flow velocities typical of real-world environments. To overcome this limitation, recent research has increasingly pivoted toward the integration of nonlinear mechanisms, specifically multi-stable structures and nonlinear energy sinks (NES), to broaden the operational bandwidth and maximize energy conversion efficiency.

A possible strategy to enhance VIV energy extraction involves engineering multi-stable restoring forces that trigger high-energy inter-well oscillations. For instance, Huang & Zhong (2023) investigated an electromagnetic bi-stable energy harvester (EBEH) with tunable negative stiffness attached to a hollow cylinder.[31] Their work demonstrated that calibrating the negative stiffness fundamentally outperforms traditional cubic stiffness, significantly amplifying the nonlinear energy transfer from flow-induced vibrations and widening the lock-in wind speed range. Pushing the boundaries of multi-stability, Zhang et al. (2024) proposed a quad-stable nonlinear piezoelectric energy harvester (PQN-PEH) that employs piecewise stiffness.[32] By utilizing magnetic repulsion alongside flexible stoppers, their design secures broadband low-frequency energy capture while critically preventing structural fatigue and damage during strong, large-amplitude resonances.

Beyond maximizing power generation, there is an engineering need to protect host structures from the potentially destructive impacts of VIV. Consequently, modern research paradigms treat energy harvesting and vibration suppression as a unified, dual-functional objective. As discussed in a comprehensive review by Huang and Yang (2023),[33] these systems operate on an "energy shunt" principle by strategically redistributing, converting, and dissipating unwanted mechanical energy into electrical power. Building upon this regenerative energy strategy, Huang (2024) designed a multi-stiffness dynamic vibration absorber (NECMC-DVA) that seamlessly synergizes bistable, cubic, and linear stiffnesses. This architecture achieves remarkable transient shock robustness and targeted energy transfer (TET), acting as both a high-efficiency harvester and a dampener.[34]

Further exploring these actively controlled hybrid architectures, Huang et al. developed a bionic-dipteran magnetoelastic bi-stable dynamic vibration absorber (BDMB-DVA).[35] Their study confirmed that active, tunable stiffness configurations can maintain broadband targeted energy transfer and continuous vibration mitigation under multi-source harmonic disturbances. Similarly, Huang et al. expanded on this by introducing a low-frequency, two-stage hybrid vibration isolator that combines an NES with a negative stiffness spring.[36] This integrated approach exhibited superior vibration isolation and a broader working bandwidth compared to traditional linear absorbers, highlighting the exceptional kinetic energy capture capabilities of bistable NESs.

Collectively, these advancements establish that marrying multi-stable nonlinear oscillators with tunable stiffness mechanisms represents a state-of-the-art framework for next-generation VIV energy extractors. By successfully coupling broadband flow-induced energy harvesting with robust structural vibration mitigation, these integrated systems provide a highly reliable foundation for powering wireless sensor networks in complex fluid-structure environments.

Despite the promise of ocean current energy, its large-scale deployment presents significant technical and environmental challenges. These include ensuring structural durability under complex hydrodynamic loads, maintaining ecosystem compatibility, and achieving cost-effective installation and maintenance. However, recent advancements in marine energy technologies and computational tools are paving the way toward overcoming these barriers, making ocean current energy an increasingly viable clean energy solution.

Numerical modeling plays a critical role in the design and optimization of ocean energy harvesters by enabling performance prediction under varying environmental conditions. Advanced computational tools allow researchers to simulate interactions between ocean currents and energy-harvesting devices, assess structural integrity, and optimize efficiency. Computational fluid dynamics (CFD) is widely used to analyze flow behavior, turbulence, and pressure distributions around turbines and other harvesting systems.[37,38] When coupled with real-world data, CFD enables the identification of optimal deployment strategies, reducing development costs and maximizing energy output.[39,40] It also facilitates the evaluation of novel concepts, such as biomimetic turbines inspired by marine organisms, prior to physical prototyping.[41-42]

High-performance computing (HPC) resources have further accelerated the modeling process, enabling the simulation of large-scale arrays and multi-physics interactions within practical timeframes. When integrated with machine learning algorithms, these tools can incorporate adaptive learning techniques to optimize design parameters in real time.[43] Moreover, digital twins, known as virtual counterparts of physical systems, are increasingly used to monitor and predict device behavior under dynamic marine conditions, enabling a continuous feedback loop from design to deployment.[44]

A holistic approach that integrates experimental research, numerical modeling, and digital engineering is essential for the continued advancement of ocean current energy technologies. The synergy between physical testing and simulation enables iterative improvements in design, while digital tools support the transition from laboratory-scale development to commercial application. Initiatives such as the European Union's Horizon 2020 MaRINET2 program exemplify the impact of collaborative efforts in accelerating innovation through shared knowledge, infrastructure, and resources.[45] Building upon these advancements, this article focuses on the development of a novel technology for harvesting ocean current energy, with particular emphasis on vortex-induced motion systems and advanced numerical modeling. By addressing key challenges and exploring emerging opportunities, the study aims to contribute to the growing body of knowledge that underpins the global shift toward clean, renewable energy.

Recent work by Guðlaugsson et al. (2025) introduced a comprehensive Feasibility Assessment Framework (FAF) for VIV-based energy harvesters, applied to a DIY small-scale device deployed in a river channel in Ljubljana, Slovenia.[46] Their framework integrates technical performance, economic cost-benefit analysis, environmental life-cycle assessment, and social acceptance evaluation. The present work complements their study by focusing on a larger-scale ocean current application with a fundamentally different device configuration (the dual-cylinder VIMEC concept) and by employing a stochastic economic assessment methodology that provides probabilistic LCOE estimates rather than deterministic values.

The scientific contributions and novelty of the present work are threefold:

(1) A novel enhanced VIV energy converter concept (VIMEC): Unlike conventional VIV energy harvesters that rely on a single isolated cylinder operating within the narrow lock-in bandwidth (typically Ur = 4–8), the VIMEC system employs a secondary upstream cylinder to deliberately trigger a combined VIV-galloping response. This extends the operational velocity range significantly beyond the lock-in regime, addressing one of the principal limitations of existing VIV-based energy converters. While prior studies have investigated tandem cylinder arrangements for energy harvesting (e.g., the VIVACE device[23]), the specific offset configuration employed in VIMEC, designed to create a converging channel and asymmetric flow, represents a distinct approach to enhancing the flow-induced motion.

(2) Integrated numerical-experimental validation at realistic scale: the present study provides both high-fidelity 2D RANS-based CFD simulations and towing-tank experiments at SINTEF Ocean for a common VIMEC configuration, enabling direct cross-validation. This dual-method approach, conducted at a physically meaningful scale (cylinder diameter of 150 mm, Reynolds numbers up to 45,000), goes beyond the small-scale piezoelectric or laboratory-scale studies prevalent in literature. The validated numerical model then enables parametric exploration of the design space (PTO damping, boundary layer effects) that would be prohibitively expensive to explore experimentally.

(3) Stochastic economic feasibility assessment: while previous economic assessments of VIV energy harvesters have relied on deterministic LCOE calculations, as recently highlighted by Guðlaugsson et al. (2025), who reported average LCOE values of 6.3 - 6.5 EUR/kWh for a DIY VIV-EH device using a Feasibility Assessment Framework (FAF), the present work introduces a probabilistic Monte Carlo approach that explicitly quantifies the economic uncertainty envelope.[46] This stochastic methodology captures the asymmetric risk profile characteristic of early-stage marine energy technologies and provides confidence intervals rather than single-point estimates, offering a more rigorous basis for investment decision-making. Our analysis complements the comprehensive multi-dimensional feasibility framework proposed by Guðlaugsson et al. (2025), which integrates technical, economic, environmental, and social assessments, by providing a deeper probabilistic treatment of the economic dimension specifically tailored to the higher-power VIMEC system targeting ocean current deployments.

MATERIALS AND METHODS

Vortex induced motion energy harvesting device concept

The Vortex-Induced Motion Energy Converter (VIMEC) is an energy-harvesting device that operates based on enhanced FIV. Its core component is a primary oscillating structure, typically a cylinder, aligned with its main axis perpendicular to the incoming fluid flow, as illustrated in Figure 1A & B.

The secondary smaller cylinder positioned upstream and in proximity to the primary cylinder serves multiple fluid-dynamic functions that collectively enhance the energy harvesting capability. First, the converging channel formed between the two cylinders acts as a nozzle, locally accelerating the flow and increasing the dynamic pressure impinging on the primary cylinder. This acceleration effect increases the effective Reynolds number in the gap region, promoting stronger vortex shedding. Second, the wake generated by the secondary cylinder introduces periodic velocity perturbations into the flow approaching the primary cylinder. These perturbations act as a forcing mechanism that can synchronize with and amplify the natural vortex shedding of the primary cylinder, particularly when the spacing ratio is tuned appropriately. Third, the geometric asymmetry created by the offset positioning of the secondary cylinder generates a persistent asymmetric pressure distribution around the primary cylinder. This asymmetry is the key enabler of the galloping response: as the primary cylinder oscillates, the relative position of the gap changes, modulating the asymmetric forces in a manner that sustains and amplifies the motion rather than damping it. The combination of these three mechanisms: flow acceleration, wake forcing, and geometric asymmetry; produces the characteristic large-amplitude response that distinguishes VIMEC from conventional single-cylinder VIV devices.

This controlled geometric configuration triggers a coupled dynamic response, combining VIV with galloping-like oscillations. Unlike an isolated cylinder, which exhibits pure VIV, the VIMEC system achieves large-amplitude, sustained oscillations through the synergistic interaction of these two mechanisms, depending on flow conditions and system parameters.

The kinetic energy from the oscillating primary cylinder is converted into usable energy via a Power Take-Off (PTO) system. The PTO can be implemented in various forms, including a linear electric generator offering direct conversion without mechanical transmission losses, a rotational electromechanical generator requiring a motion rectification mechanism but benefiting from mature generator technology, or a positive displacement pump for hydraulic energy storage. The selection of the PTO type will depend on the target deployment scale, oscillation frequency and amplitude characteristics, and maintenance accessibility constraints. The parametric damping study presented in results provides the fundamental performance envelope within which any specific PTO system must operate.

The primary cylinder is mounted on a resilient suspension system that allows motion in one or two degrees of freedom relative to a fixed frame. Key system parameters, such as suspension stiffness, can be tuned to match the natural frequency of the structure with the target flow regime for optimal energy extraction. Moreover, spanwise splitter plates are attached to the cylinder to enhance coherence in vortex shedding along its length.

Experimental methodology

The technology verification experiments were conducted at SINTEF Ocean main towing tank shown in Figure 1C-E.[47] This facility features a 260 m long basin with a 10.5 m breadth and variable water depths, with sections of 5.6 m and 10.0 m being relevant to this study (tank layout detailed in Figure 1C). A dedicated test rig, specifically designed for this investigation and based on a pendulum principle (Figure 1D), supported a 1.0 m active length test cylinder between end plates. The pendulum, measuring 5.17 m from its upper universal joint to the cylinder's bottom end plate, was engineered to allow coupled motions in both in-line (IL) and cross-flow (CF) directions relative to towing. Suspension springs were integrated into the rig, located 1.33 m below the universal joint. Two distinct cylindrical aluminum models were utilized: a bare cylinder for baseline data, and the VIMEC oscillator configuration. Parameters of the experimental setup are listed in Table S1.

The towing carriage velocity was continuously monitored. Spring forces were measured by four force transducers co-located with the springs (1.33 m below the universal joint) with sampling frequency of 200 Hz. System vibrations were recorded by three accelerometers with sampling frequency of 200 Hz: a 3-component unit 0.67 m above the test cylinder's midpoint, another 3-component unit at the rig's top connection point, and a 1-component unit on the cylinder's upper end plate. High-fidelity 6-DOF motion data were acquired using a Qualisys optical tracking system, with four markers on a T-shaped frame 0.67 m above the cylinder's midpoint, sampling at 50 Hz; this system also defined the VIMEC model's orientation and provided redundant motion measurements. An underwater camera provided qualitative visual documentation of cylinder vibrations. Primary cylinder displacements were derived through numerical integration of accelerometer data, with band-pass filter applied between 0.5 Hz and 5 Hz. These calculated displacements showed good agreement with the Qualisys system measurements, except at the highest towing speeds where surface wave generation compromised optical tracking accuracy.

Prior to towing, system identification was performed through decay tests. Initial tests in air, with the rig assembled with and without the test cylinder using various spring arrangements, established structural damping ratios and natural frequencies. These results guided the selection of the final spring

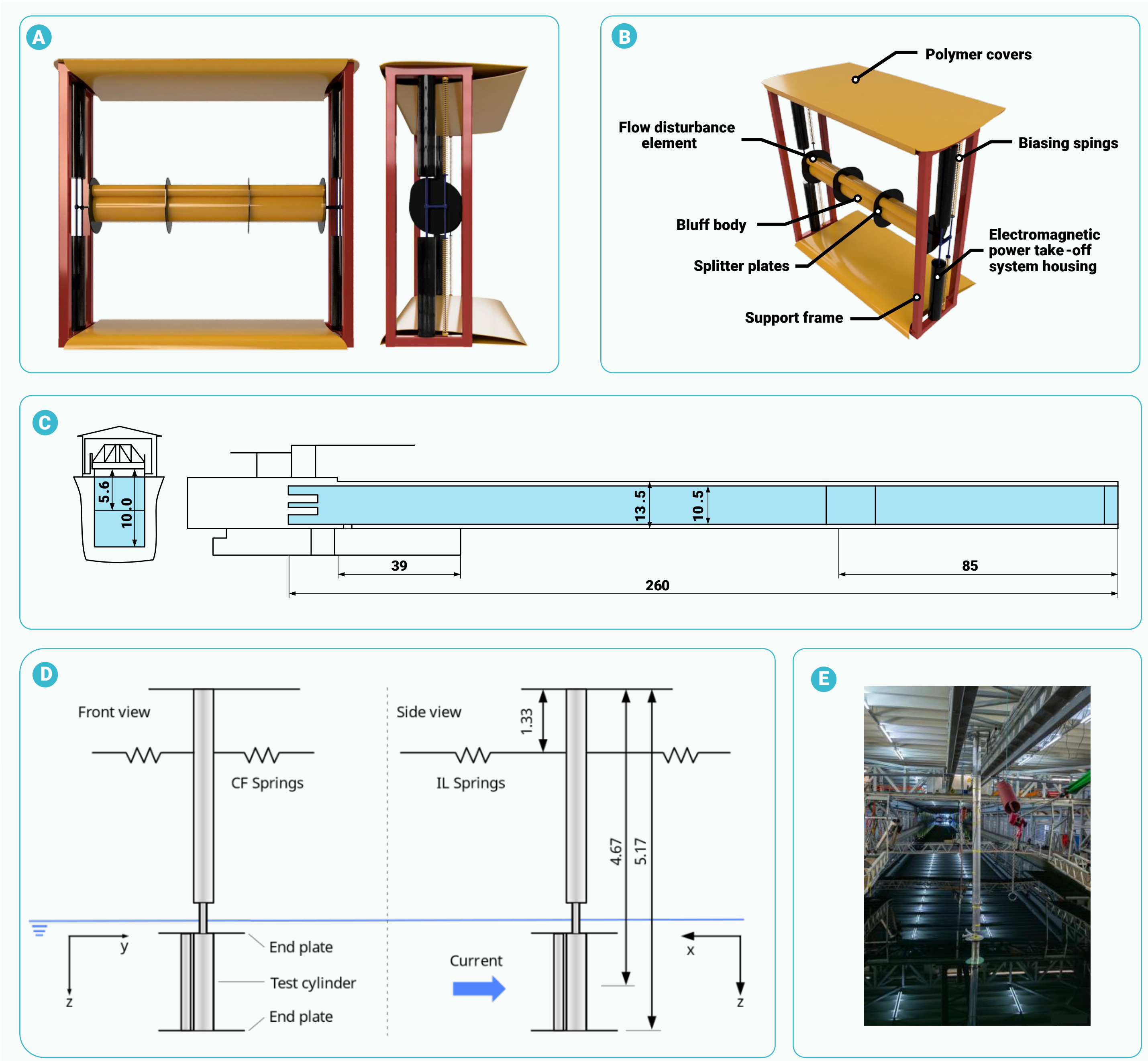

Figure 1. (A) & (B) Overview of the VIMEC device concept And experimental verification of VIMEC oscillator: (C) details of the towing tank and, (D) schematic and (E) photography of the pendulum test rig allowing tracking the 2DOF VIV response.

setup to target a system mass ratio (m^*) of approximately 2.0 and a natural frequency (f_n) near 1.0 Hz in still water, assuming an added mass coefficient (C_a) of 1.0. Subsequent decay tests in still water confirmed the hydrodynamic natural frequencies and damping for both cylinder models. The main experimental program consisted of free oscillation tests conducted while towing the models. In total, the test matrix comprised 34 runs: the bare cylinder underwent 4 decay tests and 16 free oscillation tests (including repetitions), while the VIMEC configuration was subjected to 2 decay tests and 12 free oscillation tests (including repetitions).

Numerical methodology

The present numerical model employs the finite volume method to solve two dimensional Reynolds Averaged Navier Stokes equations:[48]

$$\frac{\partial u_i}{\partial x_i} = 0, \tag{1}$$

$$\frac{\partial u_i}{\partial t} + u_j \frac{\partial u_i}{\partial x_j} = -\frac{1}{\rho}\frac{\partial P}{\partial x_i} + v\frac{\partial^2 u_i}{\partial x_j^2} - \frac{\partial \tau_{ij}}{\partial x_j}, \tag{2}$$

$$\tau_{ij} = \overline{u_i' u_j'} \tag{3}$$

where $i, j = x, y$ are streamwise and wall-normal directions, respectively; u_x, u_y are the time averaged flow velocity components corresponding to directions x and y, respectively; ρ is the density of the fluid; P is the dynamic pressure; τ_{ij} is the Reynolds stress tensor. The $k-\omega$ shear stress transport (SST) turbulence model is used in present study to as turbulence closure.[49] The dynamic behavior of the oscillator is described by a set of equations of motion of a rigid body:

$$m\frac{\partial^2 x}{\partial t^2} + c\frac{\partial x}{\partial t} + kx = F_x(t), \tag{4}$$

$$m\frac{\partial^2 y}{\partial t^2}+c\frac{\partial y}{\partial t}+ky=F_y(t),\tag{5}$$

where x is the displacement in IL direction, y is the displacement in CF direction, c is the structural damping, m is the mass of structure, k is the structural stiffness, in the present study set to equal value in both the IL and CF directions, F_x and F_y are the fluid forces acting in IL and CF directions, respectively. The damping ratio ζ is defined as:

$$\zeta=\frac{c}{2\sqrt{km}},\tag{6}$$

Equation for the mass ratio m^* yields:

$$m^*=\frac{m}{m_d},\tag{7}$$

where m_d is the mass of displaced fluid.

Reduced velocity formula yields:

$$U_r=\frac{u}{f_n D},\tag{8}$$

where f_n is the structure's natural frequency in still water.

$$f_n=\frac{1}{2\pi}\sqrt{\frac{k}{m}}\tag{9}$$

Lift (C_L) and drag (C_D) coefficients could be expressed by following formulas:

$$C_L=\frac{F_y}{\frac{1}{2}u^2\rho DL},\tag{10}$$

$$C_D=\frac{F_x}{\frac{1}{2}u^2\rho DL},\tag{11}$$

where L is the length of the bigger cylinder in span wise direction.

The computational domain measures 40D × 20D (where D is the cylinder diameter), with the cylinder positioned 10D downstream of the inlet. Figure 2 provides an overview of the computational domain and boundary conditions.

To establish the reliability of the numerical model, a series of sensitivity studies is first conducted. The results of grid density and time-step sensitivity analyses for flow around a stationary cylinder at $Re=1.31\times10^4, \delta=0.48$ are summarized in Table S2 and Table S3, respectively. Based on the sensitivity studies mesh density M3 and maximum Courant number, $C_{o,max}$ = 0.5 are selected for the subsequent simulations. The model is validated against the experimental data by Lei et al. (1999) investigating flow around the near-wall cylinder at Re from 1.30×10^4 to 1.45×10^4 and various gap ratios.[50] A reasonable agreement is found between the present numerical model and the experimental data as presented in Table S4. In general, the present numerical model slightly underpredicts the drag and lift coefficients at small gap ratios.

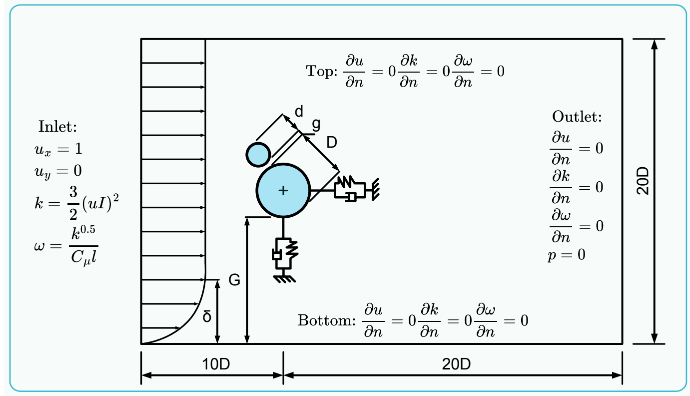

Figure 2. (A) Schematic diagram of the computational domain and imposed boundary conditions and (B) an overview of the computational mesh.

Then, the model is applied to simulate the VIMEC oscillator replicating the experimental runs described in previous section. A total of 16 cases are simulated, replicating the experimental flow conditions across the full velocity range of the towing tank test. The structural stiffness (k_i) is tuned to match the reduced velocities (U_r) used in the experiments, covering a range of $2.94 < U_r < 16.72$, which corresponds to an experimental Reynolds number range of $3.66\times10^4 < Re < 1.4\times10^5$. Other model parameters are also aligned with the parameters reported in Wu (2020): the mass ratio m*=2.0, the large cylinder diameter D = 1 m, the small cylinder diameter d = 0.5 m, gap between cylinders G = 0.1 m, the angular position of the small cylinder α = 67.5°, and the damping ratio ζ = 1%. Figure 3 presents comparison of the predicted normalized cross-flow vibration amplitudes, $\left(\frac{A_y}{D}\right)$, and normalized in-line vibration amplitudes, $\left(\frac{A_x}{D}\right)$, with the experimental measurements. The predicted $\frac{A_y}{D}$ values agree reasonably well with the experimental data across the entire tested U_r range. The numerical model overpredicts $\frac{A_y}{D}$ and $\frac{A_x}{D}$ values for U_r< 12 and underpredicts them for 15 < U_r< 17. Despite these discrepancies the model performance is assumed as sufficiently accurate for practical engineering applications.

RESULTS

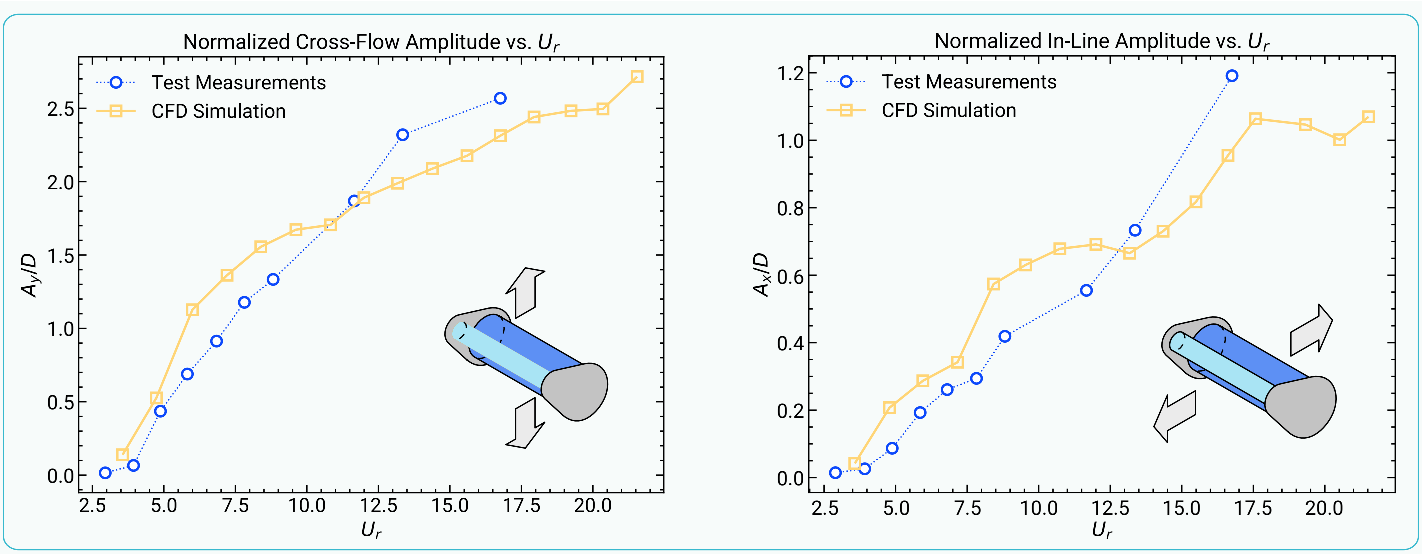

Figure 3. Comparison of the present numerical results with the present experimental test data.

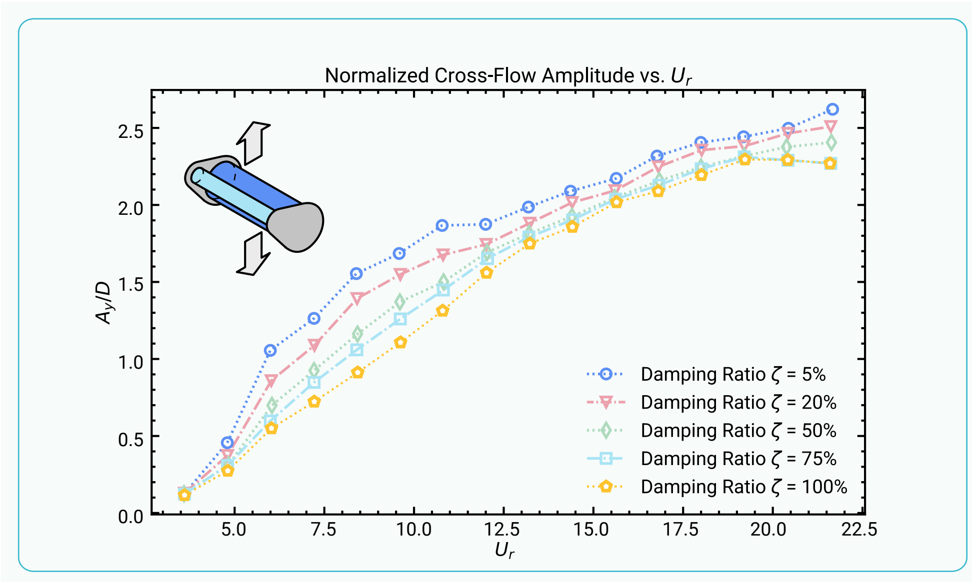

Figure 4. Effect of damping (PTO load) on hydrodynamic response of the oscillator.

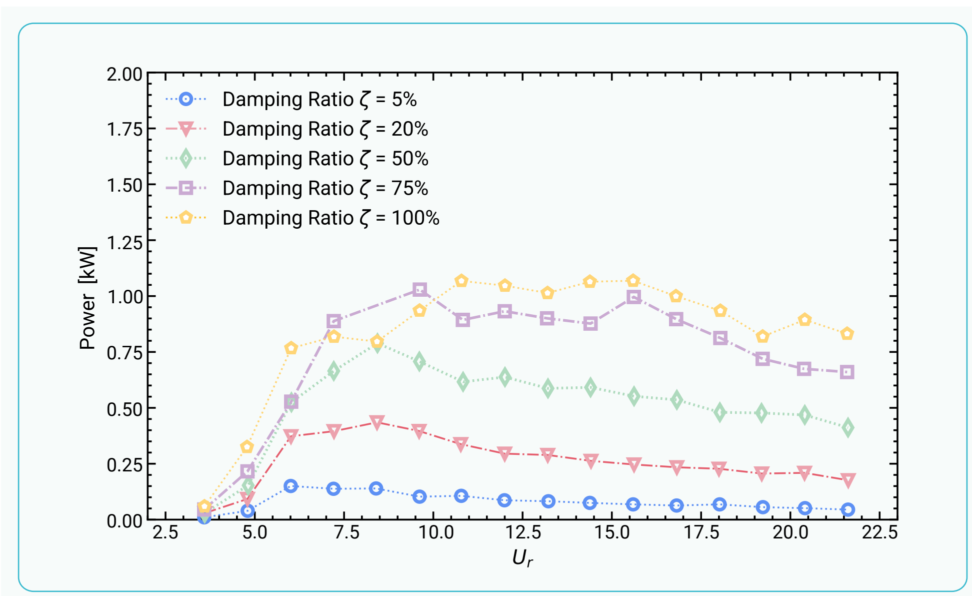

Figure 5. Effect of damping (PTO load) on the time averaged mechanical power production.

Parametric studies and economical potential

Influence of PTO damping and sensitivity to incoming flow boundary layer thickness. Oscillations of a cylinder due to the alternating lift force can be utilized to extract power from the fluid flow. Power extraction is modeled through damping in the system, representing the power take-off (PTO) mechanism. For cylinder displacement y(t), the instantaneous power extracted by the damper is:

$$P_{FIV}(t) = c\dot{y}(t)^2 \tag{12}$$

where c is the structural damping coefficient and $\dot{y}(t)$ is the cylinder velocity. For simplicity the electromagnetic damping in the following analysis is assumed to be constant. The relationship between damping and power extraction presents an inherent trade-off. Figure 4 demonstrates that increasing the damping ratio progressively suppresses the cross-flow vibration amplitude across the entire reduced velocity range. At $U_r = 10$, for instance, the normalized amplitude decreases from approximately $A_y/D = 1.9$ at $\zeta = 5\%$ to $A_y/D = 1.4$ at $\zeta = 100\%$, a reduction of roughly 26%. This suppression effect is most pronounced in the VIV-dominated region ($U_r < 10$), where the cylinder motion is more sensitive to changes in system damping. In the galloping-dominated regime ($U_r > 15$), the amplitude curves converge, indicating that the galloping instability mechanism is more robust against damping variations.

Since the oscillation amplitude fluctuates between cycles, the instantaneous power output varies accordingly. Following Soti et al. (2018),[51] time-averaged power is computed over a statistically stationary portion of the vibration time series. Figure 5 reveals the non-monotonic relationship between damping and power extraction. Here the predicted power output is based on the oscillator with dimensions of D = 1 m, L = 2 m and maximum flow velocity U_{max} = 2 m/s. The power efficiency of the converter can be defined as the ratio of the power damped by the power take off system to the theoretical power contained in the flow projected on the oscillator area:

$$\varepsilon = \frac{\overline{P_{FIV}}}{P_{max}} = \frac{\frac{1}{T}\int_T P_{FIV}(t)}{\frac{1}{2}\rho U^3 DL} \tag{13}$$

In the present case the $P_{max} = 8.2$ kW, and the efficiency of the system in the best case is approximately $\varepsilon = 14.6\%$.

Despite exhibiting the largest amplitudes, the $\zeta = 5\%$ case produces negligible power output (< 0.2 kW across all U_r), as the low damping coefficient fails to extract significant energy from the motion. Conversely, the $\zeta = 75\%$ and $\zeta = 100\%$ cases achieve peak power outputs exceeding 1.0 kW near $U_r = 10$, demonstrating that optimal power extraction requires balancing amplitude reduction against increased energy dissipation rate.

The dynamic response of the VIMEC oscillator exhibits distinct regimes as a function of reduced velocity and PTO damping. In the VIV-dominated range (Ur = 4 - 7), the oscillation frequency locks onto the natural frequency of the structure (f/fn ≈ 1), with cross-flow amplitudes reaching A/D ≈ 0.7–1.2 depending on the damping level. The phase angle between the fluid force and cylinder displacement transitions from approximately 0° (in-phase, below resonance) to approximately 180° (out-of-phase, above resonance) through the lock-in region, consistent with classical VIV behaviour. In the galloping-dominated range (Ur > 8), the oscillation frequency decreases below the natural frequency as the amplitude grows, and the force-displacement phase relationship becomes more complex due to the combined VIV-galloping mechanism. Increasing PTO damping progressively suppresses the vibration ampli-

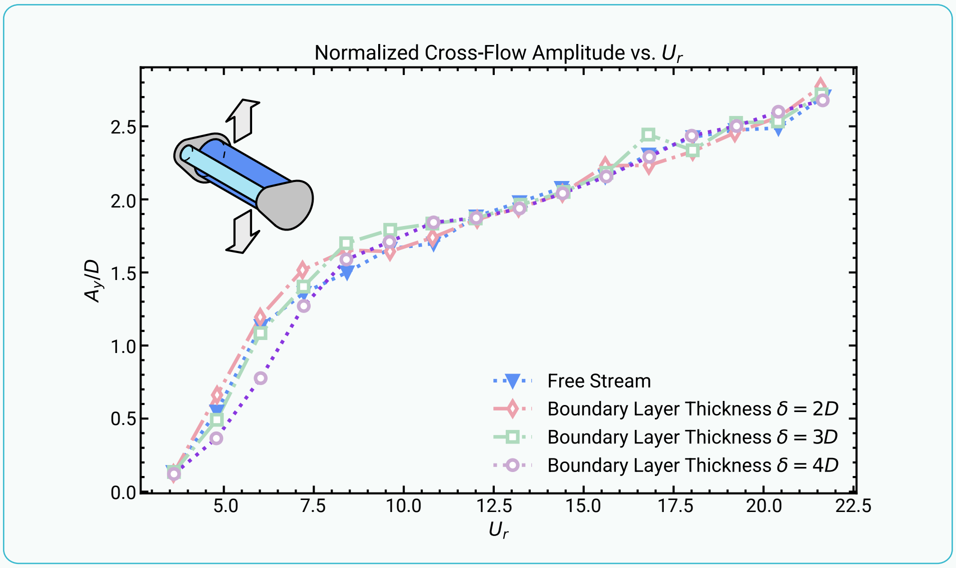

Figure 6. Effect of bottom boundary layer thickness on hydrodynamic response of the oscillator.

tude across all reduced velocities but shifts the peak response to slightly higher Ur values, as the added damping effectively increases the total system damping and modifies the resonance condition. These trends are evident in Figure 4 and are consistent with the fundamental energy balance: at optimal damping, the energy extracted by the PTO matches the maximum energy that the fluid can transfer to the structure, resulting in the power peak observed near Ur =10 in Figure 5.

The effect of boundary layer thickness on cross-flow vibration amplitude is presented in Figure 6. The sheared inflow has minimal impact on overall oscillator performance, with notable differences confined to the VIV-dominated range ($3 < U_r < 10$). Within this region, increasing boundary layer thickness generally reduces the observed cross-flow amplitudes, attributable to the reduced effective flow velocity and modified vortex shedding characteristics in the sheared profile. For boundary layer thicknesses $\delta = 2D$and $\delta = 3D$, localized amplitude enhancement relative to the uniform flow case is observed near $U_r \approx 8$, possibly due to favorable interaction between the shear profile and the lock-in mechanism. In the galloping-dominated regime ($U_r > 15$), all cases collapse onto essentially the same response curve, confirming that galloping is relatively insensitive to upstream velocity gradients.

The influence of boundary layer thickness on VIV response can be understood through the modification of the approaching velocity profile and the associated vortex dynamics. In a uniform flow, symmetric vortex shedding generates balanced alternating lift forces on the cylinder. However, when a boundary layer is present, the velocity gradient across the cylinder span introduces asymmetry in the flow field. The lower portion of the cylinder, immersed in the slower-moving region of the boundary layer, experiences reduced local Reynolds numbers and weaker vortex shedding compared to the upper portion exposed to higher velocities. This velocity gradient has several consequences: (i) if the boundary layer thickness is large compared to cylinder diameter the effective reduced velocity becomes significantly different from the nominal reduced velocity based on the free stream flow velocity; (ii) the asymmetric pressure distribution modifies the mean lift force, introducing a steady transverse force component that affects the oscillation equilibrium position; and (iii) the turbulence intensity, which is inherently higher within the boundary layer, promotes earlier transition of the shear layers separating from the cylinder surface, leading to a narrower wake and reduced coherence of vortex shedding. These combined effects explain the observed reduction in cross-flow vibration amplitude within the VIV-dominated range (Ur < 7) for thicker boundary layers, as shown in Figure 6. Notably, in the galloping-dominated range (Ur > 8), the boundary layer influence diminishes because the galloping mechanism is primarily driven by aerodynamic instability associated with the effective angle of attack of the oscillating body, which is less sensitive to the incoming velocity profile.

Levelized cost of energy (lcoe) assessment. To quantify the economic uncertainty inherent in both early-stage prototyping and future commercial scaling, the Levelized Cost of Energy (LCOE) is evaluated using a stochastic Monte Carlo simulation approach.[52] Unlike static deterministic calculations, this method assigns probability distributions to key stochastic parameters, enabling the derivation of confidence intervals for financial performance.

The standard LCOE formulation employed in the simulation is defined as:

$$LCOE = \frac{\sum_{t=1}^{n} (I_t + M_t)(1+r)^{-t}}{\sum_{t=1}^{n} E_t (1+r)^{-t}} \tag{14}$$

where I_t represents investment expenditures (CAPEX) in year t, M_t denotes operations and maintenance (OPEX) costs, E_t is the electricity generation, r is the discount rate, and n is the operational lifetime. The annual electricity generation incorporates both capacity factor and performance degradation:

$$E_t = P_{\text{rated}} \times CF \times 8760 \times (1-d)^{t-1} \tag{15}$$

where P_{rated} is the rated capacity (kW), CF is the capacity factor, and d is the annual degradation rate. To capture the asymmetric risk profile characteristic of engineering projects, where cost overruns occur more frequently than cost savings, capital and operational expenditures are modeled using log-normal distributions.[53,54] CAPEX inputs are derived from prototype fabrication costs (2.5 million NOK for the 5 kW benchmark unit), corresponding to a cost of approximately 50 000 $/kW which similar to reference prototype costs 31 000 – 49 000 $/kW recommended by NREL Reference Model Project.[55] The assumed standard deviation for CAPEX distributions σ = 0.25 reflects ±30% uncertainty typical of TRL 4–6 technologies.[55] Fixed operations and maintenance (O&M) costs are based on the review of published data for prototype and pilot tidal energy projects and are assumed to be 2% of CAPEX annually (1000 $/kW/year). Variable O&M costs, representing unscheduled maintenance events, are modeled with a gamma distribution to capture the right-skewed nature of stochastic failure-driven expenditures. The capacity factor is modeled with a beta distribution bounded by physical limits ($0 < CF \leq 1$), appropriate for representing natural resource variability in tidal energy applications.[57] Annual performance degradation accounts for biofouling, marine corrosion, and mechanical wear. A truncated normal distribution with mean 0.5% per year prevents physically unrealistic negative values while permitting accelerated degradation scenarios up to 1.5% per year under harsh marine conditions. For system lifetime, the discrete distribution explicitly captures three scenarios: 10% probability of 15 years lifetime corresponding to early decommissioning due to technical failures or market conditions, 60% probability of standard 20 years design life, 30% probability of life extension with major component refurbishment up to 25 years. The discount rate follows triangular distribution with lower, mode and upper bound set to 4%, 9.4%, and 13%, respectively. The values represent scenarios from subsidized demonstration project rates with government-backed financing (r = 4%) to commercial projects with technology risk premium (r = 13%). IRENA (2023) reports similar ranges of 2.6–5.0% for mature markets and 8–10% for emerging technologies. The analysis is performed using the probabilistic model and executing N = 50,000 simulations.[58]

The LCOE obtained by Monte Carlo simulation is presented in Figure 7. The analysis indicates a median LCOE (P_{50}) of 989 $/MWh, with a mean of 1028 $/MWh. The positive skewness implied by the mean exceeding the median is evident in the LCOE distribution histogram. The P_{10} - P_{90} confidence interval spans 683 to 1424 $/MWh, representing 80% probability band. The coefficient of variation (CV = 29.1%) indicates moderate relative uncertainty, typical

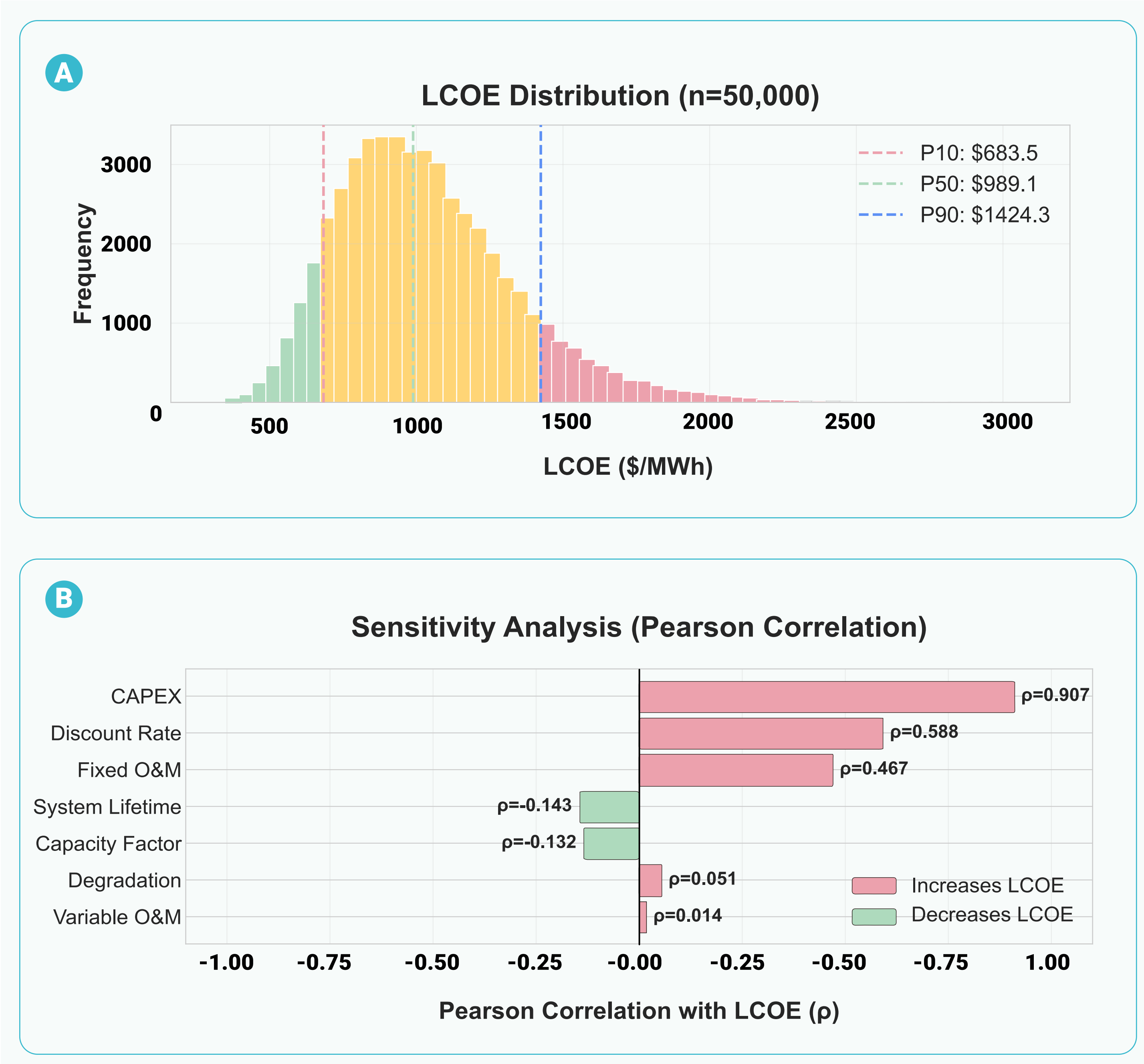

Figure 7. Results of Monte Carlo simulations and resulting LCOE distribution (Model parameters detailed in Table S5).

for early-stage renewable energy technologies where both technical and market parameters remain inadequately constrained. Pearson correlation analysis (Figure 8) reveals a clear hierarchy of cost drivers. CAPEX dominates LCOE variability with $\rho = 0.907$, indicating that 82.2% of LCOE variance is attributable to capital cost uncertainty alone. This near-linear relationship, visible in the CAPEX–LCOE scatter plot, confirms that CAPEX reduction should be the primary focus of cost optimization efforts. The discount rate, despite its mathematical prominence in the LCOE denominator, shows weaker correlation ($\rho = 0.588$) than CAPEX and contributes approximately 34.6% of explained variance when considered independently. Nevertheless, for capital-intensive renewable technologies, securing favorable financing terms remains a significant lever for improving project economics. Fixed O&M costs exhibit moderate correlation ($\rho = 0.467$), contributing approximately 21.8% of explained variance when considered independently. Notably, capacity factor and system lifetime exhibit negative correlations with LCOE ($\rho \approx -0.14$), as expected from the LCOE formulation where these parameters appear in the denominator. Variable O&M and degradation rate show negligible sensitivity, indicating that refinement of these inputs would minimally impact overall uncertainty reduction.

The current prototype-phase LCOE of approximately 1.0 \$/kWh substantially exceeds grid electricity prices, a result characteristic of bespoke fabrication at experimental scale where economies of scale remain unrealized. However, this analysis establishes a verified quantitative baseline against which future optimization strategies can be evaluated. Pathway analysis incorporating learning curve effects and industrial scaling indicates that achieving an LCOE target of 0.3 \$/kWh, competitive for diesel displacement applications, requires reducing specific CAPEX below 8000 \$/kW. Given the dominant sensitivity of LCOE to capital costs ($\rho = 0.90$), this target is attainable through manufacturing standardization, supply chain optimization, and cumulative deployment experience without requiring fundamental technological breakthroughs. The VIMEC generator is therefore assessed as economically viable when strategically positioned for Blue Economy applications and

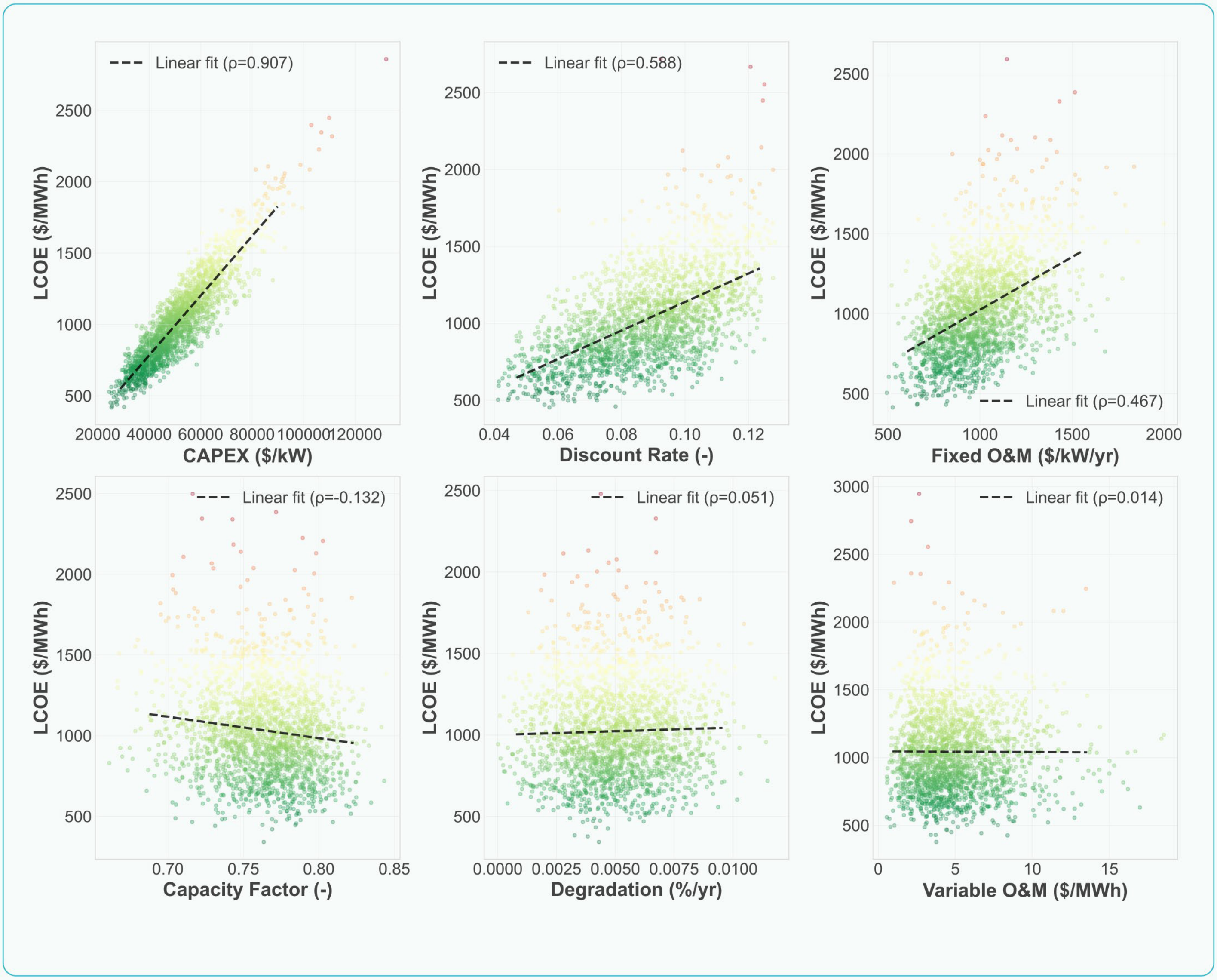

Figure 8. Stochastic Monte Carlo analysis parameter correlation with predicted LCOE.

remote microgrid markets, where incumbent diesel generation costs typically range from 0.25 – 0.50 $/kWh. Direct competition with centralized utility grids remains premature at current technology readiness levels.

The economic efficiency of the VIMEC system is strongly dependent on the prevailing flow velocity at the deployment site, through its influence on the capacity factor and annual energy production. Based on the parametric results, the power output follows a cubic relationship with flow velocity ($P \propto U^3$) modulated by the efficiency curve of the oscillator. At the optimal reduced velocity ($Ur \approx 8$), the system achieves peak efficiency of approximately 14.6%, corresponding to a power output exceeding 1.0 kW for the present configuration. At lower flow velocities (e.g., 0.5 m/s), the reduced power output (scaling with U^3) would increase the LCOE substantially, potentially by a factor of 8 compared to the baseline case at 1.0 m/s. Conversely, sites with higher mean current velocities (e.g., 1.5–2.0 m/s) would benefit from significantly higher capacity factors and proportionally lower LCOE values. This strong velocity dependence underscores the importance of careful site selection for commercial VIMEC deployments, with sites featuring sustained current velocities above 1.0 m/s being most favourable for economic viability. This finding is consistent with the observations of Guðlaugsson et al. (2025),[46] who reported that the LCOE of DIY VIV-based energy harvesters deployed in a Slovenian river channel ranged from 3.4 to 10.6 Euro/kWh depending on the flow velocity, further confirming the critical role of site hydrodynamics in determining economic feasibility.

To illustrate the practical potential of VIMEC deployment, we consider the characteristics of several well-documented ocean current sites. The Gulf Stream off the southeastern United States features sustained current velocities of 1.0–2.5 m/s,[5] which fall well within the operational envelope of the VIMEC system. At these velocities, the present VIMEC configuration would operate in the favourable galloping-dominated regime with power outputs of 1.0–3.0 kW per unit. Similarly, tidal channels such as those in the Bay of Fundy (Canada) or the Pentland Firth (UK), with peak velocities exceeding 3.0 m/s, represent high-energy sites where arrays of VIMEC devices could provide competitive power generation.

CONCLUSION

The present work leads to several important conclusions. Firstly, the numerical model predictions show reasonable agreement with experimental test results, confirming that the present numerical method is suitable for early stages of engineering design where costs and iteration speed over multiple concepts is important. Second, the device has shown it can operate consistently well even when the boundary layer thickness varies significantly, indicating it can be deployed across the water column including placement on the seabed without deteriorating the performance. A key outcome of the present study underlines the importance of the galloping-type response. This type of response allows VIMEC device to function effectively with a wider variety of damping ratios and reduced velocities compared to devices limited to a pure VIV response. Because of this extended operational range, VIMEC shows promising potential as an energy harvesting device that could be successfully deployed in many different settings. The LCOE analysis indicates that direct competition with centralized utility grids remains premature at current technology readiness levels. On the other hand, the present concept seems economically viable when strategically positioned for Blue Economy applications and remote microgrid markets. Future investigations should consider fully coupled fluid-structure-electromagnetic models to capture potential nonlinear interactions between the generator load characteristics and the hydrodynamic response, particularly the effect of velocity-dependent electromagnetic damping on the cylinder oscillation dynamics.

REFERENCES

1. Thennakoon T.M.T.N., Hewage H.T.M., Sandunika D.M.I., et al. (2023). Harnessing the power of ocean energy: A comprehensive review of power generation technologies. *J. Res. Technol. Eng.* **4**:73–102.
2. International Energy Agency (2021). Global energy review 2021. *IEA*. Available online.
3. Flores P. and Mendoza E. (2025). A fuzzy logic technique for the environmental impact assessment of marine renewable energy power plants. *Energies* **18**:272. DOI:10.3390/en18020272
4. Sadoughipour M., VanZwieten J. and Tang Y. (2025). Drifter-based global ocean current energy resource assessment. *Renew. Energy* **244**:122576. DOI:10.1016/j.renene.2025.122576
5. Haas K., Fritz H.M., French S.P., et al. (2013). Assessment of energy production potential from ocean currents along the United States coastline. *Report*. DOI:10.2172/1093367.
6. Dodo Y. and Ochi F. (2023). Demonstration test of ocean current turbine system for reliability and economic performance evaluation. *IHI Eng. Rev.* **56**.
7. Guo C., Sheng W., De Silva D.G., et al. (2023). A review of the levelized cost of wave energy based on a techno-economic model. *Energies* **16**:2144. DOI:10.3390/en16052144
8. Gu Y., Zou T., Liu H., et al. (2024). Status and challenges of marine current turbines: A global review. *J. Mar. Sci. Eng.* **12**:884. DOI:10.3390/jmse12060884
9. Barua A. and Rasel M.S. (2024). Advances and challenges in ocean wave energy harvesting. *Sustain. Energy Technol. Assess.* **61**:103599. DOI:10.1016/j.seta.2023.103599
10. Su X., Chen J., Yuan L., et al. (2025). Current status of development and application of ocean renewable energy technology. *Sustainability* **17**:5648. DOI:10.3390/su17125648
11. Boretti A. and Castelletto S. (2025). Advancements and challenges in tidal stream and oceanic current turbines: An overview of current technologies and future prospects. *Mar. Dev.* **3**:10. DOI:10.1007/s44312-025-00054-5
12. Roberts M., Nieuwenhuys C. and Guastella L. (2016). Circulation of shelf waters in the KwaZulu-Natal Bight, South Africa. *Afr. J. Mar. Sci.* **38**:S7–S21. DOI:10.2989/1814232X.2016.1175383
13. Wardhana W., Keniraras N., Pratama R.S., et al. (2021). Hydrodynamics performance analysis of vertical axis water turbine using CFD approach. *IOP Conf. Ser. Earth Environ. Sci.* **698**:012022. DOI:10.1088/1755-1315/698/1/012022
14. Xu P., Hong M., Li H., et al. (2025). Vortex-driven nanogenerators for marine energy harvesting. *Phys. Fluids* **37**:027133. DOI:10.1063/5.0250873
15. Zhu H., Chen Q., Tang T., et al. (2023). Flow structures around a circular cylinder with bilateral splitter plates. *Ocean Eng.* **269**:113547. DOI:10.1016/j.oceaneng.2022.113547
16. Wang J., Zhang C., Zhang M., et al. (2021). Enhancing energy harvesting from flow-induced vibrations of a circular cylinder using a downstream rectangular plate. *Int. J. Mech. Sci.* **211**:106781. DOI:10.1016/j.ijmesec.2021.106781
17. Margielewicz J., Gąska D., Trigona C., et al. (2026). The influence of magnet configuration on energy harvesting from torsional vibrations of drive systems. *Appl. Math. Model.* **151**:116510. DOI:10.1016/j.apm.2025.116510
18. Milne I.A., Day A.H., Sharma R.N., et al. (2016). The characterisation of the hydrodynamic loads on tidal turbines due to turbulence. *Renew. Sustain. Energy Rev.* **56**:851–864. DOI:10.1016/j.rser.2015.11.095
19. Song R., Xu P., Jiang C., et al. (2024). An experimental study on flow induced motion and energy harvesting of cylinders with different cross sections. *Front. Mar. Sci.* **11**:1461020. DOI:10.3389/fmars.2024.1461020
20. Zhang J., Xu G., Liu F., et al. (2016). Experimental investigation on the flow induced vibration of an equilateral triangle prism in water. *Appl. Ocean Res.* **61**:92–100. DOI:10.1016/j.apor.2016.10.003
21. Chang C.-C., Kumar R.A. and Bernitsas M.M. (2011). VIV and galloping of single circular cylinder with surface roughness at $3.0\times10^4\leq Re\leq1.2\times10^5$. *Ocean Eng.* **38**:1713–1732. DOI:10.1016/j.oceaneng.2011.07.013.
22. Sun H., Kim E.S., Nowakowski G., et al. (2016). Effect of mass-ratio, damping, and stiffness on optimal hydrokinetic energy conversion. *Renew. Energy* **99**:936–959. DOI:10.1016/j.renene.2016.07.056
23. Bernitsas M.M., Raghavan K., Ben-Simon Y., et al. (2006). VIVACE (Vortex Induced Vibration Aquatic Clean Energy): A new concept in generation of clean and renewable energy from fluid flow. *Proc. Int. Conf. Offshore Mech. Arctic Eng.* **2**:619–637. DOI:10.1115/OMAE2006-92645
24. Lian J., Wu Z., Yao S., et al. (2022). Experimental investigation of flow-induced motion and energy conversion for two rigidly coupled triangular prisms arranged in tandem. *Energies* **15**:8190. DOI:10.3390/en15218190
25. Xu J., Barrero-Gil A. and Velazquez A. (2016). Dual mass system for enhancing energy extraction from vortex-induced vibrations. *Int. J. Mar. Energy* **16**:250–261. DOI:10.1016/j.ijome.2016.07.004
26. Alam M.M., Moriya M. and Sakamoto H. (2003). Aerodynamic characteristics of two side-by-side circular cylinders and application of wavelet analysis on the switching phenomenon. *J. Fluid Struct.* **18**:325–346. DOI:10.1016/j.jfluidstructs.2003.07.005
27. Alam M.M., Moriya M., Takai K. and Sakamoto H. (2003). Fluctuating fluid forces acting on two circular cylinders in a tandem arrangement at a subcritical Reynolds number. *J. Wind Eng. Ind. Aerodyn.* **91**:139–154. DOI:10.1016/S0167-6105(02)00341-0
28. Alam M.M. and Sakamoto H. (2005). Investigation of Strouhal frequencies of two staggered bluff bodies and detection of multistable flow by wavelets. *J. Fluid Struct.* **20**:425–449. DOI:10.1016/j.jfluidstructs.2004.11.003
29. Tang B., Wang J., Yu X., et al. (2026). Energy harvesting of cylindrical FIV under multi prism wake. *Renew. Energy* **256**:123918. DOI:10.1016/j.renene.2025.123918
30. Rashki M.R., Hejazi K., Tamimi V., et al. (2024). Impacts of hard marine growth on 2DoF VIV-based piezoelectric energy harvesting. *Renew. Energy* **231**:120913. DOI:10.1016/j.renene.2024.120913
31. Huang X. and Zhong T. (2023). Hydrokinetic energy harvesting from flow-induced vibration of a hollow cylinder attached with a bi-stable energy harvester. *Energy Convers. Manage.* **278**:116718. DOI:10.1016/j.enconman.2023.116718
32. Zhang X., Huang X. and Wang B. (2024). A quad-stable nonlinear piezoelectric energy harvester with piecewise stiffness for broadband energy harvesting. *Nonlinear Dyn.* **112**:19633–19652. DOI:10.1007/s11071-024-10077-0
33. Huang X. and Yang B. (2023). Towards novel energy shunt inspired vibration suppression techniques: Principles, designs and applications. *Mech. Syst. Signal Process.* **182**:109496. DOI:10.1016/j.ymssp.2022.109496
34. Huang X. (2024). Exploiting multi-stiffness combination inspired absorbers for simultaneous energy harvesting and vibration mitigation. *Appl. Energy* **364**:123124. DOI:10.1016/j.apenergy.2024.123124
35. Huang X., Hua X. and Chen Z. (2025). Exploiting a novel magnetoelastic tunable bi-stable energy converter for vibration energy mitigation. *Nonlinear Dyn.* **113**:2017–2043. DOI:10.1007/s11071-024-10337-z
36. Huang X., Wang B., Huang Z., et al. (2025). A theoretical model for a low-frequency two-stage hybrid vibration isolator with a nonlinear energy sink and a negative stiffness spring. *Appl. Math. Model.* **142**:115948. DOI:10.1016/j.apm.2025.115948
37. Mejia O.D.L., Quiñones J.J. and Laín S. (2018). RANS and hybrid RANS-LES simulations of an H-type Darrieus vertical axis water turbine. *Energies* **11**:2348. DOI:10.3390/en11092348
38. Iliev R., Todorov G., Kamberov K. and Zlatev B. (2025). Evaluation of the performance of optimized horizontal-axis hydrokinetic turbines. *Water* **17**:1532. DOI:10.3390/w17101532
39. Lee C.T. (2025). Advancing marine renewable energy for island nations: Design and development of a 20 kW floating Kuroshio turbine (FKT). *J. Energy Power Technol.* **7**:017. DOI:10.21926/jept.2504017
40. Ng C.Y., Maldar N.R. and Ong M.C. (2026). Effect of diffuser inlet angles on the power and torque coefficients of a hydrokinetic turbine. *J. Offshore Mech. Arct. Eng.* **148**:012008. DOI:10.1115/1.4069635
41. Hernández Montoya E.E., Mendoza E. and Stamhuis E.J. (2023). Biomimetic design of turbine blades for ocean current power generation. *Biomimetics* **8**:118. DOI:10.3390/biomimetics8010118
42. Zhou Z., Benbouzid M., Charpentier J.-F., et al. (2017). Developments in large marine current turbine technologies: A review. *Renew. Sustain. Energy Rev.* **71**:852–858. DOI:10.1016/j.rser.2016.12.113
43. Rashid H., Hanzla M., Berghout T., et al. (2025). RegStack machine learning model for accurate prediction of tidal stream turbine performance and biofouling. *Expert Syst. Appl.* **283**:127766. DOI:10.1016/j.eswa.2025.127766
44. Katsidoniotaki E., Psarommatis F. and Göteman M. (2022). Digital twin for the prediction of extreme loads on a wave energy conversion system. *Energies* **15**:5464. DOI:10.3390/en15155464
45. European Commission (2021). European Union's Horizon 2020 MaRINET2 program. Available online. DOI:10.3030/731084.
46. Guðlaugsson B., Hocevar M., Secnik M., et al. (2026). Feasibility assessment of a DIY vortex-induced vibration energy harvester for remote and off-grid power supply. *Energy Convers. Manage. X* **30**:101755. DOI:10.1016/j.ecmx.2026.101755
47. Wu J. (2020). VIMEC test. Report No. 302005150.
48. Weller H.G., Tabor G., Jasak H. and Fureby C. (1998). A tensorial approach to computational continuum mechanics using object-oriented techniques. *Comput. Phys.* **12**:620–631. DOI:10.1063/1.168744
49. Menter F.R., Kuntz M. and Langtry R. (2003). Ten years of industrial experience with

the SST turbulence model. *Proc. Int. Symp. Turbulence Heat Mass Transfer*. 625–632.
50. Lei C., Cheng L. and Kavanagh K. (1999). Re-examination of the effect of a plane boundary on force and vortex shedding of a circular cylinder. *J. Wind Eng. Ind. Aerodyn.* 80:263–286. DOI:10.1016/S0167-6105(98)00204-9
51. Soti A.K., Zhao J., Thompson M.C., et al. (2018). Damping effects on vortex-induced vibration and implications for power extraction. *J. Fluid Struct.* 81:289–308. DOI:10.1016/j.jfluidstructs.2018.04.013
52. Lee C.-Y. and Ahn J. (2020). Stochastic modeling of the levelized cost of electricity for solar PV. *Energies* 13:3017. DOI:10.3390/en13113017
53. Touran A. and Wiser E.P. (1992). Monte Carlo technique with correlated random variables. *J. Constr. Eng. Manag.* 118:258–272. DOI:10.1061/(ASCE)0733-9364(1992)118:2(258
54. Wall D.M. (1997). Distributions and correlations in Monte Carlo simulation. *Constr. Manag. Econ.* 15:241–258. DOI:10.1080/014461997372980
55. Jenne D.S., Yu Y.-H. and Neary V. (2015). Levelized cost of energy analysis of marine and hydrokinetic models. *Proc. Mar. Energy Technol. Symp.*
56. Neary V.S., Previsic M., Jepsen R.A., et al. (2014). Methodology for design and economic analysis of marine energy conversion technologies. *Report*.
57. National Renewable Energy Laboratory (2024). Annual Technology Baseline: Financial Cases & Methods. *NREL*. https://atb.nrel.gov/electricity/2024/.
58. International Renewable Energy Agency (2023). The cost of financing for renewable power. *IREA*.

FUNDING AND ACKNOWLEDGMENTS

The authors acknowledge the support from FORNY program (NFR309075) financed by the Research Council of Norway.

AUTHOR CONTRIBUTIONS

Muk Chen Ong: Conceptualization, Methodology, Software, Validation, Formal Analysis, Investigation, Resources, Writing-Original Draft, Writing-Review & Editing, Visualization, Project Administration, Funding Acquisition.
Marek Jan Janocha: Conceptualization, Methodology, Software, Validation, Formal Analysis, Investigation, Resources, Writing-Original Draft, Writing-Review & Editing, Visualization, Project Administration, Funding Acquisition.

DECLARATION OF INTERESTS

Muk Chen Ong is an Editorial Board member of The Innovation Energy and was blinded from reviewing or making final decisions on the manuscript. Peer review was handled independently of this member and their research group. The other authors declare no conflicts of interest.

DATA AND CODE AVAILABILITY

Data are available from the corresponding author upon reasonable request.

SUPPLEMENTAL INFORMATION

It can be found online at: https://doi.org/10.59717/j.xinn-energy.2026.100153